KSME

Springer

Journal of Mechanical Science and Technology 36 (10) 2022

Original Article
DOI 10.1007/s12206-022-0929-5

Keywords:
· Planetary reducer
· Novel abnormal cycloidal gear
· Meshing principle
· Transmission characteristics
· Stress analysis

Correspondence to:
Shanming Luo
smluo@jmu.edu.cn

Citation:
Mo, J., Luo, S., Fu, S., Chang, X. (2022). Meshing principle and characteristics analysis of an abnormal cycloidal internal gear transmission. Journal of Mechanical Science and Technology 36 (10) (2022) 5165~5179.
http://doi.org/10.1007/s12206-022-0929-5

Received April 21st, 2022
Revised June 15th, 2022
Accepted June 28th, 2022

† Recommended by Editor Hyun-Kyu Kim

Meshing principle and characteristics analysis of an abnormal cycloidal internal gear transmission

Jingyu Mo[1,2], Shanming Luo[2], Shengping Fu[2] and Xuefeng Chang[2]

[1]School of Aerospace Engineering, Xiamen University, Xiamen 361005, China, [2]College of Marine Equipment and Mechanical Engineering, Jimei University, Xiamen 361021, China

Abstract A novel 2K-H internal meshing abnormal cycloidal gear (ACG) planetary reducer is proposed to tackle the rotor vector (RV) reducer problems, such as complex over-positioning structure, high manufacturing and assembly accuracy requirements. The composite tooth profile of epicycloid-involute-hypocycloid is adopted as the tooth profile of the reducer. The aim of this study was to investigate the meshing principle of such gear and evaluate its transmission characteristics. The meshing principle of tooth profile of the ACG is described. According to the gear geometry theory, the mathematical model of conjugate tooth profile of ACG pair was derived based on the contact path. And the influence of design parameters on the ACG tooth profile were also carried out. Moreover, the non-interference condition of the ACG pair was derived, and then meshing characteristics of the ACG pair were analyzed by numerical example, such as contact ratio, sliding ratio, and meshing efficiency. The bending and contact stresses of the ACG pair were also evaluated by comparing with those of involute pair. The results show that, the ACG has good transmission characteristics, such as small sliding ratio, high transmission efficiency. Compared with the involute gear, the bending and contact stresses of the ACG are reduced. The study lays a theoretical foundation for the optimization design of the ACG and the improved reliability of the ACG reducer.

1. Introduction

The rotor vector (RV) reducer has been widely applied in many industrial areas for power transmission, such as robots, CNC machine and automobile assembly, due to its low noise, compact design, high transmission efficiency and accuracy [1, 2]. However, two problems for RV reducer application exist [3, 4]: (1) Three crankshafts simultaneously act on the cycloidal gear, belonging to the over-positioning structure. Theoretically, half of the cycloidal needle teeth mesh at the same time, resulting in high requirements for the mechanical properties and machining accuracy of the parts, which then greatly increases the difficulty of machining and assembly of the reducer. (2) The pressure angle of the cycloid gear pair changes widely, and the dynamic load of the system is large, which leads to abnormal wear or rupture of the boom bearing and affects the service life of the reducer.

Researchers have done considerable research to deal with the problems mentioned above, including meshing characteristics, mechanical design, and development of new type of tooth profile. Wu et al. [5] analyzed the influence of manufacturing and assembly tolerance on the transmission error of the RV reducer. Results show that the pitch errors of pin position and cycloid teeth were the main factors affecting transmission errors. Han et al. [6] investigated the influence of clearance, machining error and assembly error on the transmission accuracy of the reducer. Results show that the error of cycloid wheel and pinwheel crankshaft has the greatest influence on the transmission accuracy. These studies are contributing to improving the transmission performance of the reducer, but cannot fundamentally solve the problems in the manufacture and assembly of the reducer. In view of the limits in the structure of RV reducer, re-

searchers attempted to develop a new reducer to realize the RV reducer performance. Lin et al. [7] introduced a design method for cycloid gear reducer based on graph analysis, which provides a theoretical basis for developing the reducer. Gorla et al. [8] proposed a cycloid reducer with outer gear ring and cylindrical roller installed on the planetary wheel. Its structural characteristics and mechanical properties were also investigated. Blagojevic et al. [9] proposed a cycloid reducer, which set the phase difference of gear pair to 180° to solve the counterweight problem of gear drive. Hsieh et al. [10] proposed a new reducer with pinwheel fixed and internal gear output, and verified its superiority through theory and simulation. Sun et al. [11] proposed a new single-stage cycloid-pin reducer, and also discussed profile modification and lost motion. Results show that the reducer has a small lost motion. Park et al. [12] replaced cycloid teeth with involute to solve the sensitivity of cycloidal drive to center distance, and the low-cost manufacturing of precision reducer was realized. Lin et al. [13] proposed a new transmission of planetary gear with the simultaneous internal meshing of the sun gear and ring for the problem of uneven loading of planetary gear transmission, and verified the correctness of the transmission principle and motion law by using virtual prototype technology. Xu et al. [14] proposed a new reducer based on ball drive, and verified that the reducer could achieve high working efficiency through theoretical and experimental studies. The above research shows that developing a new type of reducer can improve the efficiency and performance of the machine.

Furthermore, gear tooth profile is a fundamental element to determine the transmission performance of a gear drive, and also affect the output performance of the transmission device. To meet the different functional requirements of gear transmission and improve the mechanical performance, researchers have done much useful work in the design and performance analysis of a new tooth profile. Wang et al. [15] proposed a cycloid internal meshing tooth profile with an arc contact path, and carried out its geometrical and numerical analysis. The results show that the tooth has a high contact ratio and load capacity. Xu et al. [16] proposed an external meshing tooth profile with a combined internal and external cycloid, and also studied the effect of design parameters on the sliding ratio. The tooth profile has a low sliding ratio and uniform wear. Peng et al. [17] developed an arc-tooth-trace cycloid composite tooth profile for the limitations of conventional tooth profile in terms of load carrying capacity, and also analyzed its meshing principle and characteristics. Zhou et al. [18] proposed a new tooth profile suitable for a gear pump, which is composed of arc-involute-arc. A mathematical model of the tooth profile was established, and its performance was studied by experimental test. Chen et al. [19] proposed a novel cycloid transmission with double contact lines. The equations of tooth profile and contact path were derived, and its meshing characteristics were also carried out by theoretical analysis. Therefore, the above research indicates that the development of new type of tooth profile is helpful to improve the performance of gear transmission.

Our research group proposes a novel type of abnormal cycloidal gear (ACG) reducer [20], 2K-H internal meshing planetary gear transmission, as shown in Fig. 1(a). This mechanism consists of an input shaft with a crank, a planetary wheel, an internal gear and an adaptor with cylindrical pins. Compared with RV reducer, the proposed reducer eliminates the needle tooth and special output structure, and the manufacturing and assembly difficulty of the reducer are also reduced. Meanwhile, the three crank shafts are changed into a single crank shaft and pin, which contributes to alleviating the over-positioning problem of the RV reducer. In our previous research work [21], the transmission scheme, working principle and transmission ratio of ACG reducer were studied. The results show that the proposed reducer can achieve high transmission ratio and large transmission torque. However, the contact ratio and load capacity of the gear in ACG reducer are lower than that of RV reducer. The relative sliding between the conjugate tooth profiles affects the smooth operation of the reducer. In view of this, a new type of composite tooth profile is proposed to further improve the load capacity and meshing performance of the ACG reducer. The important feature of the proposed gear is that the tooth profile is composed of epicycloid, involute and hypocycloid segments,

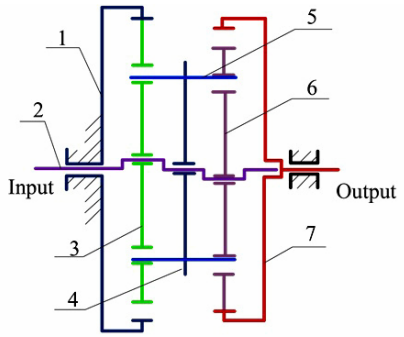

1—Case 2—Input shaft 3—Abnormal cycloid gear 4—Adaptor
5—Pin 6—Abnormal cycloid gear 7—output gear

(a)

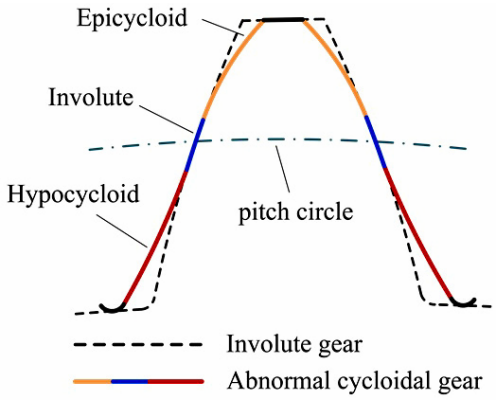

(b)

Fig. 1. ACG reducer and its tooth profile: (a) transmission scheme; (b) comparison of tooth profile.

named abnormal cycloidal gear (ACG), as shown in Fig. 1(b). Therefore, we carried out some analysis, and elaboration of the tooth profile of the ACG is given in this paper.

The main objective of the work was to investigate the meshing principle of the ACG and analyze its meshing characteristics. The generate principle and contact path of tooth profile of the ACG are described. The equation of conjugate tooth profiles of ACG pair is derived based on the contact path. And the transmission characteristics are also carried out by numerical examples. The contact and bending stress of the ACG pair are calculated and compared with that of the conventional involute drive, which shows the good characteristic of this novel ACG. The study provides a guidance for the engineering application of ACG reducer in the future.

2. Generate principle and contact path equation of the ACG tooth profile

In this section, the generate principle of tooth profile of the ACG is described in Sec. 2.1. The equation of contact path of the ACG is established in Sec. 2.2.

2.1 Generate principle

Different from conventional tooth profile of involute and cycloid, the tooth profile of ACG is composed of three segments: epicycloid, involute, and hypocycloid. The first segment refers to the involute at the top and bottom of the pitch curve, and the second and third segments are epicycloid and hypocycloid tangent to the two ends of the involute, as shown in Fig. 2.

The generate principle of tooth profile of the ACG is as follows:

(1) Point *b* is fixed on a rolling circle with radius r_{a1}. When the rolling circle purely rolls along the outside of the pitch circle, the trajectory curve *ab* at point *b* generates the tooth profile of epicycloid segment.

(2) Point *c* is fixed on a rolling circle with radius r_{f1}. When the rolling circle rolls purely along the outside of the pitch circle, the trajectory curve *cd* at point *c* generates the tooth profile of hypocycloid segment.

(3) The tooth profile involute segment is generated past the pitch point M and its endpoints are connected to points *b* and *c* of tooth profile of epicycloid and hypocycloid segments, respectively. Among them, at the points *b* and *c*, the pressure angle of involute segment is equal to that of epicycloid and hypocycloid segments, respectively.

Half of the tooth profile is generated through the above method. It is then mirrored with the tooth thickness central axis to finally obtain a complete tooth profile of the ACG.

As mentioned above, the tooth profile of the ACG has the advantages of both cycloid and involute tooth profile:

(1) Low sensitivity to center distance error. Compared with the conventional cycloid tooth profile, the ACG tooth profile has a constant pressure angle near the pitch circle, so that when the center distance changes slightly, the ACG pair can still achieve a fixed transmission ratio, the sensitivity to the center distance error can be reduced [22].

(2) Small sliding ratio, high contact strength. Compared with the involute tooth profile, both ends of the ACG tooth profile are cycloid, and its sliding ratio is theoretical lower than that of the involute drive. Moreover, since the mesh of the ACG is convex-to-concave, this kind of gear has good meshing performance, which can increase the contact area and reduce the contact stress of the tooth.

2.2 Equation of contact path

The tooth profile design using contact path can break through the limitation of large calculation in the traditional tooth profile design process, make the tooth profile design more flexible, and meet a variety of predetermined meshing performance or function requirements [23]. Herein, based on the gear mesh theory, a method to design the conjugate tooth profile of the ACG is proposed by constructing a contact path.

The fixed coordinate system Σ_f- $X_f O_f Y_f$ is connected to the pitch point M, as shown in Fig. 3. The contact path of the ACG pair can be defined by the trajectory curve of the contact point

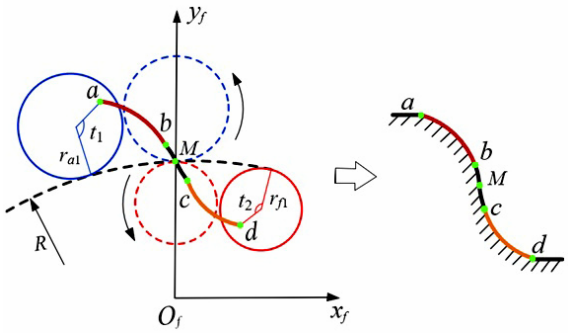

Fig. 2. Generate principle of the ACG tooth profile.

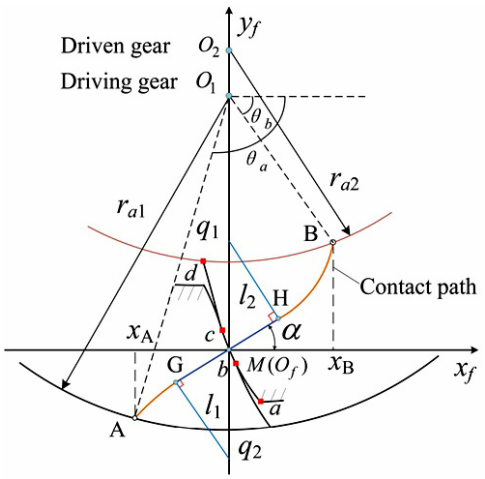

Fig. 3. Contact path of the ACG drive.

of the conjugate tooth profile. According to gear mesh theory [24], the contact path of the ACG can be divided into three segments:

(i) In the first quadrant of Σ_f, the arc $\widehat{BH}$ is used to create the dedendum curve of the driving gear, namely, hypocycloid tooth profile.

(ii) In the third quadrant of Σ_f, the arc $\widehat{GA}$ is used to create the addendum curve of the driving gear, namely, epicycloid tooth profile.

(iii) Between the $\widehat{BH}$ and $\widehat{GA}$, the straight line $\overline{\mathrm{GH}}$ is used to create a curve near the pitch point of the driving gear, namely, involute tooth profile.

Note that the $\overline{\mathrm{GH}}$ is tangent to the $\widehat{BH}$ and $\widehat{GA}$ at the points H and G, respectively. According to the geometric relationship, given the parameters of $\widehat{BH}$ and $\widehat{GA}$, the length and angle of the line $\overline{\mathrm{GH}}$ are determined. So, when the epicycloid segment of the addendum and the hypocycloid segment of the dedendum are given, the position of the involute segment is also determined.

To establish the mathematical model of the conjugated tooth profile for the ACG drive, its contact path needs to be constructed first. Assuming that r_{a1} and r_{a2} are the radius of the addendum circle of the driving gear and driven gear, respectively. A (x_A, y_A) is the meshing exit point, B (x_B, y_B) is the meshing entry point, α is the angle between the $\overline{\mathrm{GH}}$ and positive x axis, l_{Mq1} is the distance between the center q_1 of the arc $\widehat{BH}$ and pitch point M, l_{Mq1} is the distance between the center q_2 of the arc $\widehat{GA}$ and pitch point M. And they have

$$\begin{cases} l_{Mq1} = \mu_1 r_1 \\ l_{Mq2} = \mu_2 r_2 \end{cases} \tag{1}$$

where μ_1 and μ_2 are dimensionless coefficients, the pitch circle radius of the driving gear is r_1 and of the driven gear is r_2.

(1) Segments $\overline{MH}$ and $\overline{MG}$

According to the geometric characteristics of the contact path of the ACG, the equation of line $\overline{MH}$ is described in Σ_f as:

$$r^1_{f-L}(\lambda_1) = \begin{bmatrix} x^1_{f-L} \\ y^1_{f-L} \\ 1 \end{bmatrix} = \begin{bmatrix} \lambda_1 \cos\alpha \\ \lambda_1 \sin\alpha \\ 1 \end{bmatrix} \tag{2}$$

where λ_1 is the independent variable, the upper and lower indices of r represent quadrants and coordinate systems, respectively.

Similarly, the equation of line $\overline{MG}$ can be expressed in Σ_f as

$$\mathbf{r}^3_{f-L}(\lambda_2) = \begin{bmatrix} x^3_{f-L}(\lambda_2) \\ y^3_{f-L}(\lambda_2) \\ 1 \end{bmatrix} = \begin{bmatrix} -\lambda_2 \cos\alpha \\ -\lambda_2 \sin\alpha \\ 1 \end{bmatrix} \tag{3}$$

where λ_2 is the independent variable.

(2) Segment $\widehat{BH}$

The equation of $\widehat{BH}$ is described in Σ_f as:

$$\begin{bmatrix} x^1_{f-C}(\varphi_1) \\ y^1_{f-C}(\varphi_1) \\ 1 \end{bmatrix} = \begin{bmatrix} \mu_1 r_1 \cos\alpha \sin\varphi_1 \\ \mu_1 r_1 (1 - \cos\alpha \cos\varphi_1) \\ 1 \end{bmatrix} \tag{4}$$

where φ_1 is the rotation angle of the driving gear.

To ensure continuity and smoothness of transmission during gear meshing, the $\overline{MH}$ is equivalent to the tangent vector of $\widehat{BH}$ at the point H, and is obtained to be

$$\frac{dy^1_{f-L}/d\lambda_1}{dx^1_{f-L}/d\lambda_1} = \frac{dy^1_{f-C}/d\varphi_1}{dx^1_{f-C}/d\varphi_1}. \tag{5}$$

Substituting Eqs. (2) and (4) into Eq. (5), and it can be simplified as

$$\tan\alpha = \tan\varphi_1. \tag{6}$$

Since the radius l_2 of $\widehat{BH}$ is perpendicular to the line $\overline{MH}$, the maximum value of the λ_1 can be obtained based on the geometric relationship,

$$\lambda_{1\max} = \mu_1 r_1 \sin\alpha. \tag{7}$$

(3) Segment $\widehat{GA}$

Likewise, the equation of arc $\widehat{GA}$ is obtained by

$$\begin{bmatrix} x^3_{f-C}(\varphi_2) \\ y^3_{f-C}(\varphi_2) \\ 1 \end{bmatrix} = \begin{bmatrix} -\mu_2 r_2 \cos\alpha \sin\varphi_2 \\ -\mu_2 r_2 (1 - \cos\alpha \cos\varphi_2) \\ 1 \end{bmatrix} \tag{8}$$

and then the maximum value of the parameter λ_2 in $\overline{MG}$ can be obtained as:

$$\lambda_{2\max} = -\mu_2 r_2 \sin\alpha \tag{9}$$

Based on Eqs. (1)-(9), the mathematical model of contact path of ACG can be obtained by the MATLAB software.

3. Mathematical model of the ACG pair based on the contact path

In this section, the mathematical model of conjugate tooth profile for the ACG pair is established based on contact path. The influence of the design parameters on the tooth profile of the ACG is also analyzed by the numerical examples.

3.1 Coordinate systems

The generation of the ACG tooth profile is based on the given contact path. Fig. 4 shows the internal meshing coordi-

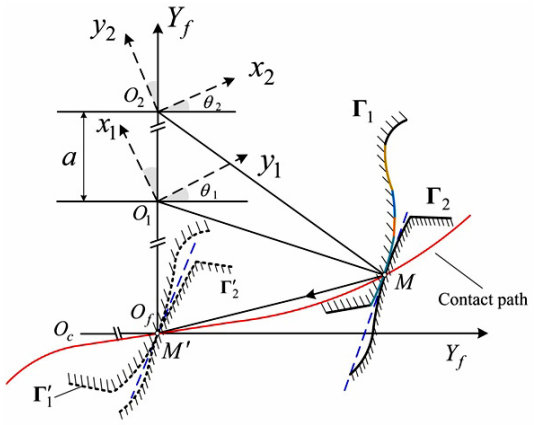

Fig. 4. Coordinate systems of the ACG drive.

nate systems of the ACG pair, where member 1 is the driving gear and member 2 is the driven gear. The moving coordinate systems Σ_1-$X_1O_1Y_1$ and Σ_2-$X_2O_2Y_2$ are rigidly connected to the centers of driving gear and driven gear, respectively. The center of the driving gear is O_1 and of the driven gear is O_2.

Assuming that a is center distance, i_{12} is transmission ratio (subindexes 1 and 2 denote driving gear and driven gear, respectively), the tooth number of driving gear is z_1 and of driven gear is z_2, the rotational angular velocities of driving gear is ω_1 and of driven gear is ω_2, the rotate angle of driving gear is θ_1 and of driven gear is θ_2. Γ_1 and Γ_2 are the conjugate tooth surfaces of driving gear and driven gear, respectively.

According to the transmission ratio of the transform mechanism [24], the above parameters have the following relations:

$$i_{12}=\frac{\omega_1}{\omega_2}=\frac{\theta_1}{\theta_2}=\frac{r_2}{r_1}=\frac{z_2}{z_1}. \tag{10}$$

Through coordinate transforming, the equation of the ACG tooth profile can be described in the coordinate system Σ_i as

$$\Gamma_i^j(t,\theta_i)=\mathbf{M}_{if}(\theta_i)\cdot\mathbf{r}_f^j(t) \tag{11}$$

where Γ subscript i (i = 1 , 2) represents the gear, and superscript j represents the quadrant in the coordinate system Σ_f, j = 1, 3. M_{if} represents the coordinate transformation matrix from the coordinate system Σ_f to Σ_i, which is expressed as

$$\mathbf{M}_{if}(\theta_i)=\begin{bmatrix}\cos\theta_i & \sin\theta_i & -r_i\sin\theta_i\\ -\sin\theta_i & \cos\theta_i & -r_i\cos\theta_i\\ 0 & 0 & 1\end{bmatrix}$$

According to the theory of gearing [24], the correct meshing condition of two conjugate gears is as follows: the product of the position vector $\vec{\boldsymbol{v}}_1$ of tooth surface contact and its normal vector $\vec{\mathbf{n}}_1$ is zero. Therefore, the meshing equation of the ACG drive can be expressed as

$$f_1=\vec{\mathbf{n}}_1\bullet\vec{\boldsymbol{v}}_1=\vec{\mathbf{n}}_1\cdot\frac{d\Gamma_1}{du}\frac{du}{dt}=0. \tag{12}$$

Differentiating Eq. (12), and it can be simplified as

$$\theta_i=-\frac{(1+i)}{a}\int_0^{\varphi_1}\left[x_f'(\varphi)+\frac{y_f(\varphi)y_f(\varphi)}{x_f(\varphi)}\right]d\varphi. \tag{13}$$

Based on Eqs. (10)-(13), given the design parameters of the contact path, the tooth profile of ACG can be obtained.

3.2 Dedendum tooth profile

The contact path $\overline{MH}$ and $\widehat{BH}$ are located between the pitch circle and the dedendum circle of the driving gear. Thus, the ACG tooth profile defined by the given contact path is the addendum tooth profile from the pitch point to the tip of the gear tooth.

Substituting Eq. (2) into Eq. (11), the equation of tooth profile of involute segment in the coordinate system Σ_1 is derived as:

$$\begin{aligned}\Gamma_{1-L}^1(\lambda_1,\theta_1(\lambda_1))&=\mathbf{M}_{1f}(\theta_1)\cdot\mathbf{r}_{f-L}^1\\&=\begin{bmatrix}-r_1\sin\theta_1(\lambda_1)+\lambda_1\cos(\alpha-\theta_1(\lambda_1))\\-r_1\cos\theta_1(\lambda_1)+\lambda_1\sin(\alpha-\theta_1(\lambda_1))\\1\end{bmatrix}.\end{aligned} \tag{14}$$

In the same way, substituting Eq. (4) into Eq. (11), the equation of tooth profile of hypocycloid segment can be established by the known contact path as:

$$\begin{aligned}\Gamma_{1-C}^1(\varphi_1,\theta_1(\varphi_1))&=\mathbf{M}_{1f}(\theta_1)\cdot\mathbf{r}_{f-C}^1\\&=\begin{bmatrix}(\mu_1r_2-r_1)\sin\theta_1(\varphi_1)+\mu_1r_2\cos\alpha\sin(\varphi_1-\theta_1(\varphi_1))\\(\mu_1r_2-r_1)\cos\theta_1(\varphi_1)-\mu_1r_2\cos\alpha\cos(\varphi_1-\theta_1(\varphi_1))\\1\end{bmatrix}.\end{aligned} \tag{15}$$

Subsequently, substituting Eqs. (2) and (4) into Eq. (13), the meshing equation of the ACG pair at the addendum tooth can be expressed as:

$$\begin{cases}\theta_1(\lambda_1)=-\dfrac{\sec\alpha}{r_1}\bullet\lambda_1\\ \theta_1(\varphi_1)=\mu_1 i(\varphi_1-\alpha)+\mu_1 i\tan\alpha\end{cases}. \tag{16}$$

According to Eq. (10), the driving gear and the driven gear have the relationship as the following equation:

$$\begin{cases}\theta_1=i_{12}\theta_2\\ r_2=i_{12}r_1\end{cases}. \tag{17}$$

By replacing θ_1 and r_1 in Eqs. (14) and (15) with θ_2 and r_2, the equation of addendum tooth profile of driven gear can be obtained.

3.3 Addendum tooth profile

Likewise, the driving gear addendum profile is generated by the contact path $\overline{MG}$ and $\widehat{GA}$. Substituting Eq. (7) into Eq. (11), the equation of tooth profile of the involute segment is obtained as

$$\begin{aligned}\Gamma_{1-L}^{3}(\lambda_2,\theta_1(\lambda_2))&=\mathbf{M}_{1f}(\theta_1)\cdot\mathbf{r}_{f-L}^{3}\\&=\begin{bmatrix}-r_1\sin\theta_1(\lambda_2)-\lambda_2\cos(\alpha-\theta_1(\lambda_2))\\-r_1\cos\theta_1(\lambda_2)-\lambda_2\sin(\alpha-\theta_1(\lambda_2))\\1\end{bmatrix}.\end{aligned}\tag{18}$$

Substituting Eq. (8) into Eq. (11), the equation of tooth profile of epicycloid segment is obtained as

$$\begin{aligned}\Gamma_{1-c}^{3}(\varphi_2,\theta_1(\varphi_2))&=\mathbf{M}_{1f}(\theta_1)\cdot\mathbf{r}_{f-C}^{3}\\&=\begin{bmatrix}(-\mu_2 r_2\cos\theta_1-r_1)\sin\theta_1(\varphi_2)+\mu_2 r_1\cos\alpha\sin(\varphi_2-\theta_1(\varphi_2))\\(-\mu_2 r_2\cos\theta_1-r_1)\cos\theta_1(\varphi_2)+\mu_2 r_1\cos\alpha\cos(\varphi_2-\theta_1(\varphi_2))\\1\end{bmatrix}.\end{aligned}\tag{19}$$

Substituting Eqs. (7) and (8) into Eq. (13), the meshing equation of the ACG drive at the addendum tooth can be expressed as

$$\begin{cases}\theta_1(\lambda_2)=\dfrac{\sec\alpha}{r_1}\bullet\lambda_2\\\theta_1(\varphi_2)=\mu_2(\varphi_2-\alpha)+\mu_2\tan\alpha\end{cases}.\tag{20}$$

Based on Eq. (17), replace θ_1, r_1 in Eqs. (18) and (19) with θ_2, r_2, the equation of dedendum profile of the driven gear can be also obtained.

3.4 Influence of design parameters on the ACG tooth profile

Based on the proposed contact path, the mathematical models of ACG tooth profile can be obtained. Since the ACG tooth profile is directly related to α, μ_1, μ_2, it is necessary to analyze the influence of design parameters on the ACG tooth profile. Considering the symmetry of the gear machining tool, set $\mu = \mu_1 = \mu_2$. Given the design parameters of the ACG in Table 1, a numerical example is carried out by MATLAB software.

Figs. 5 and 6 show the effect of μ and α on the tooth profile of the ACG. The red line represents the tooth profile of epicycloid segment, the blue line represents the tooth profile of involute segment, and the green line represents the tooth profile of hypocycloid segment.

Fig. 6 shows the influence rule of μ on the tooth profile of the ACG when other parameters remain constant. The following results are obtained:

(1) The value of μ has a significant effect on the tooth profile composition of the ACG. When the value of μ is small, the profile curves of the ACG in the tip and root portions of the tooth are mainly cycloidal tooth profile. With the further increase of the μ value, the cycloidal tooth profile of the ACG in the tip and root portions gradually decreases, while the involute tooth profile gradually increases and, finally, all of them become involute tooth profile, as shown in Fig. 5(h). Therefore, to avoid the whole ACG tooth profiles to become involute, a smaller value of μ should be selected.

(2) The value of μ has a significant effect on the thickness of the tooth tip and root of the ACG. When the value of μ increases, the tooth top thickness of the ACG gradually becomes thicker, while the tooth root thickness gradually becomes thinner. That is, under the same tooth height, taking a smaller value of μ can increase the tooth root thickness and load capacity of the ACG.

(3) Comparing Figs. 5(a) and (h), it is found that the addendum thickness of the ACG is smaller than that of involute gear, and the thickness of tooth root is thicker than that of involute gear, which indicates that the load capacity of the ACG is theoretically higher than that of involute gear at the tooth root. In

Table 1. Design parameters of the ACG pair.

Parameters	Values
Modulus m (mm)	2.25
z_1	52
z_2	56
Addendum coefficient h_a^*	0.8
Tip clearance coefficient c^*	0.3

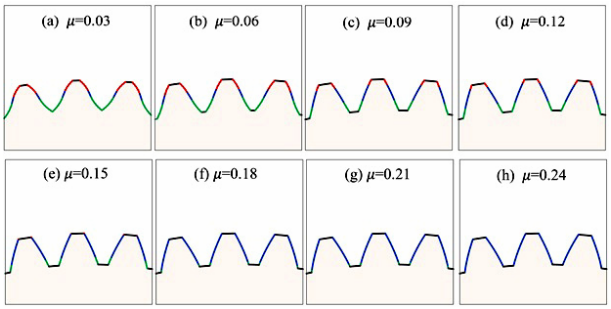

Fig. 5. Effect of μ on the tooth profile of the ACG (α = 25°).

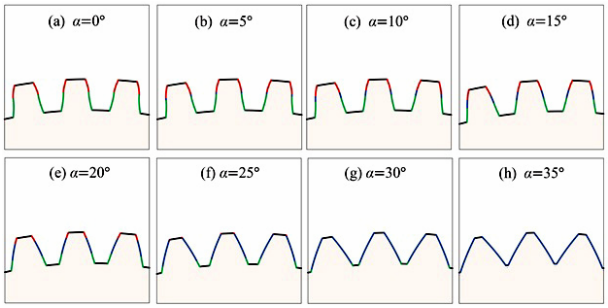

Fig. 6. Effect of α on the tooth profile of the ACG (μ = 0.15).

addition, because there is a cycloid tooth profile at the tooth tip and root, according to the gear meshing principle, the phenomenon of root cutting will not occur.

Likewise, keeping other parameters constant, the influence rule of α on the tooth profile of the ACG is shown in Fig. 6. The following results are obtained:

(1) The value of α has a significant influence on the involute tooth profile length on the ACG tooth profile. When α = 0°, the ACG tooth profile is transformed into a cycloid tooth profile, which indicates that cycloid gear is a special form of the ACG, as shown in Fig. 6(a). When the value of α is small, the involute tooth profile on the ACG tooth profile is relatively small near the pitch circle, and the ACG tooth profile of the tip and root part is mainly cycloid. With the gradual increase of the value of α, the involute tooth profile on the ACG tooth increases significantly, and eventually all of them become involute tooth profile, as shown in Fig. 6(h).

(2) The value of α has a great influence on the load capacity and service life of the ACG. With the increase of the α value, the tip thickness of the ACG tooth profile gradually decreases, and the thickness of the tooth root gradually thickens. The load capacity will be significantly improved at the tooth root, but contact ratio of the gear will be reduced, as shown in Figs. 6(a) and (d). Meanwhile, according to $F_r = F_t tan\alpha$, as the tangential force F_t is fixed, the axial force F_r increases with the increase of α . However, if the axial force is too large, the gear will have axial displacement, which will affect the normal operation of the gear and reduce the transmission efficiency and accelerate the wear of gear [25]. Therefore, considering the load capacity and service life of the ACG, a smaller value of α should be selected as far as possible.

As mentioned, α and μ have a significant influence on the tooth profile shape and composition of the ACG. However, the change of α and μ will also affect the contact path of the ACG, which leads to the contact ratio change. Therefore, to ensure the continuous transmission of the gear pair and give full play to the transmission performance of the ACG, the influence of α and μ on the tooth profile shape of the ACG should be considered in concert when designing ACG.

4. Analysis of ACG tooth profile overlapping interference

Next, the overlapping interference of tooth profile of the ACG pair is studied, and the judgment conditions of overlapping interference of tooth profile of the ACG pair are also proposed.

4.1 Overlapping interference model

If the design parameters of the internal meshing gear drive are selected improperly, the overlapping interference of the tooth profile will occur outside the meshing area, which will affect the correct meshing. The overlapping interference of the tooth profile problem also existed in the ACG pair. Hence, the design parameters such as the number of teeth, pressure angle, dimensionless coefficient, and tip height coefficient of the ACG need to be limited.

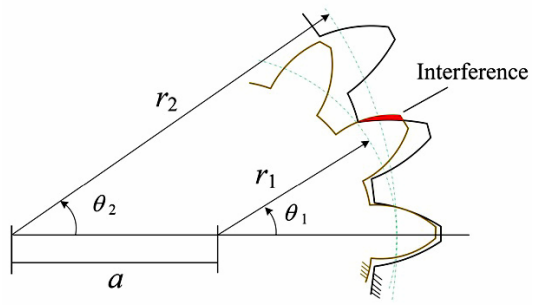

Fig. 7. Interference of overlapping tooth profile of internal gear pair.

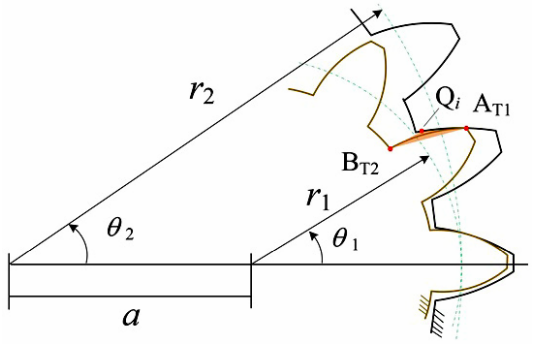

Fig. 8. ACG internal meshing tooth profile overlap.

Outside the meshing area, when the conjugate tooth profile interferes, a point on the tooth profile of the gear will enter the other gear, called the profile overlap interference phenomenon, as shown in Fig. 7. Herein, the no-interference condition is that the teeth profile of the driven gear is always kept outside of the teeth profile of the driving gear before the meshing teeth is completely separated.

Fig. 8 shows the interference phenomenon in the meshing process of the ACG pair. $Q_i(x_i, y_i)$ is a point on the profile of the driven gear, $B_{T2}(x_{T2}, y_{T2})$ is the point at the root of the driving gear tooth, and $A_{T1}(x_{T1}, y_{T1})$ is the point at the tip of the driving gear tooth. Then the equation of the area volume S of the area bounded by Q_i, B_{T2}, and A_{T1} is obtained by

$$S = (x_{T2} - x_i)(y_{T1} - y_i) - (y_{T1} - y_i)(x_{T2} - x_i) . \quad (21)$$

According to the position relation between Q_i, B_{T2} and A_{T1}, it can be determined whether the tooth profile overlapping interference occurs in the ACG pair. The method is as follows:

First, according to the design parameters of the gear, the coordinates of A_{T1} and B_{T2} on the driving gear are determined. Then, the area S is judged by substituting $Q_i(x_i, y_i)$ at any point on the driving gear into Eq. (21), that is, along the direction of tooth profile B_{T2} A_{T1}:

A) If S (B_{T2}, A_{T1}, Q_i) > 0, point Q_i is on the left side of the B_{T2} A_{T1}, and the tooth profile has no interference;

B) If S (B_{T2}, A_{T1}, Q_i) < 0, point Q_i is on the right side of the

B_{T2} A_{T1}, and the tooth profile interferes;

C) If S (B_{T2}, A_{T1}, Q_i) = 0, point Q_i is on the B_{T2} A_{T1}, and the tooth profile has no interference.

Therefore, the condition of correct meshing of the ACG pair is that the point Q_i on the profile of driven gear must satisfy min S (B_{T2}, A_{T1}, Q_i) ≥ 0.

4.2 Interference analysis

The interference judgment method of the tooth profile is validated based on numerical example. The solid models of the ACG pair are established by using the MATLAB and SOLIDWORKS software. Given the ACG pair with α = 14.5° and α = 25°, and the values of other basic design parameters are shown in Table 1. The results are shown in Fig. 9.

Fig. 9 shows the ACG internal meshing transmission model with different α. It is found that when α is 14.5°, the driving gear has tooth profile overlap interference with the driven gear, as shown in Fig. 9(a). When α is 25°, the ACG pair is in meshing without any interference, as shown in Fig. 9(b). When a pair of the ACG teeth enter into meshing, the other pair of teeth have not yet exited meshing. Thence, the necessary continuity of action can be ensured. The results show that the ACG pair without interference can be successfully designed by using the proposed method.

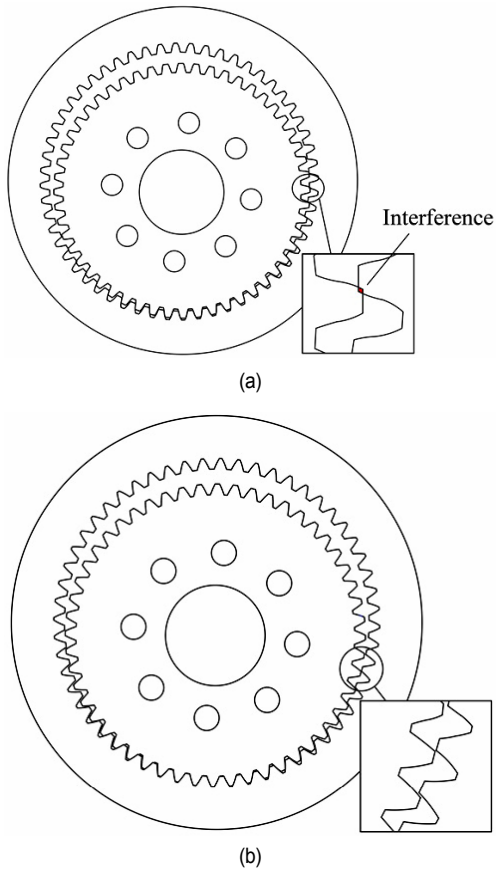

Fig. 9. Geometry model of ACG pair: (a) α = 14.5°; (b) α = 25°.

5. Meshing characteristics analysis

The meshing characteristics, such as contact ratio, sliding ratio and meshing efficiency, are the important concepts of the gear mechanism, and those are also an important index to evaluate the smoothness, accuracy and power loss of the gear drive. Therefore, it is necessary to study these meshing parameters of ACG drive to guide the gear design.

In this section, the model of meshing characteristics is established, and the influence of design parameters on the meshing characteristics of the ACG pair is also studied.

5.1 Contact ratio

(1) Contact ratio model. The continuity and smoothness of gear transmission can be ensured when the last pair of gear teeth have entered the engagement before the current pair of gear teeth are disengaged [26]. Therefore, contact ratio is an important index to measure the continuity, stability and bearing capacity of gear transmission. To ensure the continuous and smooth transmission of the ACG pair, the contact ratio must be greater than 1.

As marked in Fig. 3, there are two points (A and B) on the contact path, points A and B are the limiting meshing point at the contact path when the tooth profile of driving gear meshes with that of the driven gear. θ_b is the angle between $\overline{O_1B}$ and the positive half axis of X-axis, θ_a is the angle between $\overline{O_1A}$ and the positive half axis of X-axis. When one meshing cycle is completed, the point B moves to point A, and the amount of angle change of the driving gear is $\Delta\theta = \theta_a - \theta_b$. According to the theory of gearing, the contact ratio of the ACG is obtained by

$$\varepsilon = \frac{Z_1(\theta_a - \theta_b)}{2\pi}. \tag{22}$$

According to the geometric relation $O_1O_f + O_fA = O_1A$, we have

$$r_1 + y^3_{f-C}(\theta_a) = r_{a1}\sin(\pi - \theta_a). \tag{23}$$

Then, in ΔO_1BO_2, by the Cosine theorem of triangles, we have

$$a^2 + \left(\frac{x^1_{f-C}(\theta_b)}{\cos\theta_b}\right)^2 - r_{a2}^2 = 2a\frac{x^1_{f-C}(\theta_b)\cos(\pi/2 + \theta_b)}{\cos\theta_b}. \tag{24}$$

Based on Eqs. (23) and (24), θ_a and θ_b can be obtained, respectively, and then substituted into Eq. (22), the value of contact ratio can be also obtained.

(2) Contact ratio analysis. From Eq. (22), the contact ratio of the ACG pair is related to Z_1, Z_2, α, and μ. To analyze the contact ratio, a number of examples of ACG pair are provided

Table 2. ACG pair with different design parameters (h_a^* = 0.8 c* = 0.3 m = 3).

	α (°)	μ	Z_1	Z_2
Case a	[5 10 15 20]	0.1	40	60
Case b	20	[0.1 0.13 0.16 0.19]	40	60
Case c	5	0.1	[30 36 45 60]	90
Case d	5	0.1	40	[60 80 100 120]

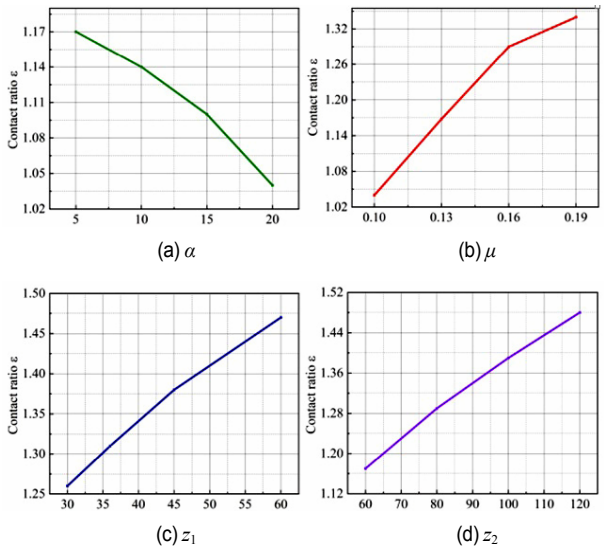

Fig. 10. Influence of design parameters on the contact ratio.

according to the parameters in Table 2.

The result of the effects of design parameters on the contact ratio of the ACG pair is shown in Fig. 10. It can be observed that the effect of design parameters on the contact ratio of the ACG is non-linear. When the α is increased, the contact ratio of the ACG pair will be decreased. When the μ, Z_1 and Z_2 is increased, the contact ratio of the ACG pair will be decreased. The main reason is that when the value of α is increased, the tip of the ACG tooth will be sharper and the number of teeth involved in the meshing will be reduced; thus the contact ratio of the ACG pair will be decreased.

5.2 Sliding ratio

(1) Sliding ratio model. In the meshing process of the ACG pair, the speed and direction of the driving gear and the driven gear are different at the contact point, which causes the two tooth surfaces to relative sliding to each other. The relative sliding is the main cause of tooth surface wear and power loss, which directly affects the transmission accuracy and durability of gear. To improve the transmission quality of the ACG, the relative sliding between two tooth surfaces should be reduced as much as possible [27]. The relative sliding between tooth surfaces is usually characterized by sliding ratio.

From meshing theory, the sliding ratio represents the relative sliding speed between the tooth profiles, which can be defined by the ratio of the relative sliding arc length of two tooth profiles to the total arc length of tooth surfaces. For the ACG pair, the equation of sliding ratio is

$$\sigma_1 = \lim_{\Delta S_1 \to 0} \frac{\Delta S_1 - \Delta S_2}{\Delta S_1} = \frac{dS_1/d\theta - dS_2/d\theta}{dS_1/d\theta} \tag{25}$$

$$\sigma_2 = \lim_{\Delta S_2 \to 0} \frac{\Delta S_2 - \Delta S_1}{\Delta S_2} = \frac{dS_2/d\theta - dS_1/d\theta}{dS_2/d\theta} \tag{26}$$

where $dS_i = d\Gamma_i/d\theta$ (i = 1, 2).

While the gear moves from the point of meshing entry to near the pitch circle, the sliding ratio for the ACG pair can be given as

$$\begin{cases} \sigma_{1-L}^1 = \dfrac{1/r_1 - 1/r_2}{1/r_1 - \sin\alpha/\lambda_1} \quad , \quad \sigma_{1-C}^1 = \dfrac{1/r_1 - 1/r_2}{1/r_1 - 1/\mu_1 r_2} \\ \sigma_{2-L}^1 = \dfrac{1/r_2 - 1/r_1}{1/r_2 - \sin\alpha/\lambda_1} \quad , \quad \sigma_{2-C}^1 = \dfrac{1/r_2 - 1/r_1}{1/r_2 - 1/\mu_1 r_2} \end{cases} . \tag{27}$$

Similarly, the sliding ratio for the ACG pair when the gear meshes from the pitch circle to the meshing out point can be given as

$$\begin{cases} \sigma_{1-L}^3 = \dfrac{1/r_1 - 1/r_2}{1/r_1 + \sin\alpha/\lambda_2} \quad , \quad \sigma_{1-C}^3 = \dfrac{1/r_1 - 1/r_2}{1/r_1 + 1/\mu_2 r_1} \\ \sigma_{2-L}^3 = \dfrac{1/r_2 - 1/r_1}{1/r_2 + \sin\alpha/\lambda_2} \quad , \quad \sigma_{2-C}^3 = \dfrac{1/r_2 - 1/r_1}{1/r_2 + 1/\mu_2 r_1} \end{cases} . \tag{28}$$

(2) Sliding ratio analysis. According to Eqs. (27) and (28) , it can be found that the sliding ratio of the ACG is related to r_1, r_2, μ, and α. To further investigate the influence rule of μ and α on the sliding ratio of the ACG pair, substituting the parameters in Tables 1 and 3 into Eqs. (27) and (28), the values of the sliding ratio of the ACG are calculated as shown in Fig. 11.

Using the previously described equations, the sliding ratio of the ACG pair is investigated. Keeping the remaining parameters constant and varying the value of α, the variation law of the sliding ratio with α is obtained, as shown in Fig. 11. The following results are obtained:

(a) For the ACG pair, the sliding ratio of the two gears in mesh is constant at both ends of the tooth profile. Near the pitch point, the sliding ratio of ACG pair decreases with an increase in α. This indicates that the value of α mainly affects the sliding ratio near the pitch circle of the ACG.

(b) Compared with the tooth profile of involute gear, the sliding ratio of tooth profile of ACG is constant, and the value of sliding ratio is smaller than that of the involute profile. Because the sliding ratio of gear is smaller, the wear of tooth surface is more uniform [28]. Therefore, the ACG pair have good wear resistance.

Similarly, keeping other parameters constant and varying the value of μ, the variation law of the sliding ratio with μ is ob-

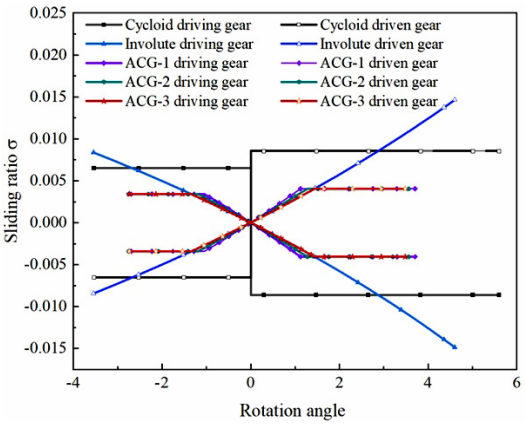

Fig. 11. Effect of α on the sliding ratio of the ACG (μ = 0.005).

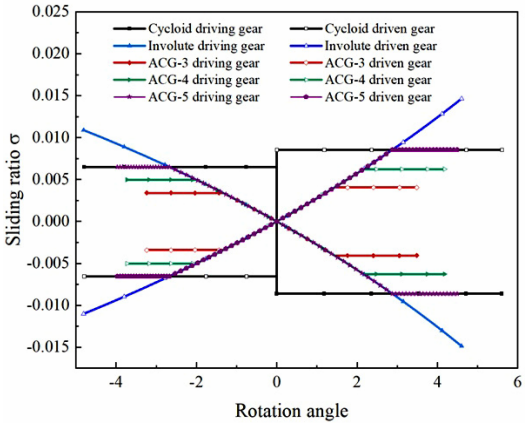

Fig. 12. Effect of μ on the sliding ratio of the ACG (α = 25°).

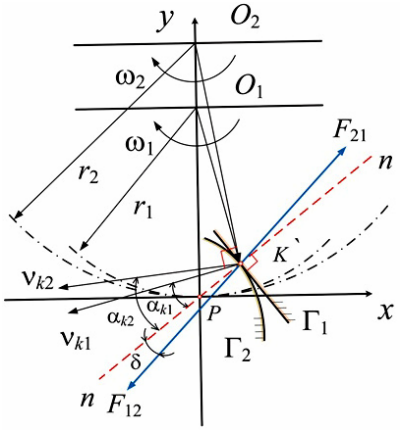

(a)

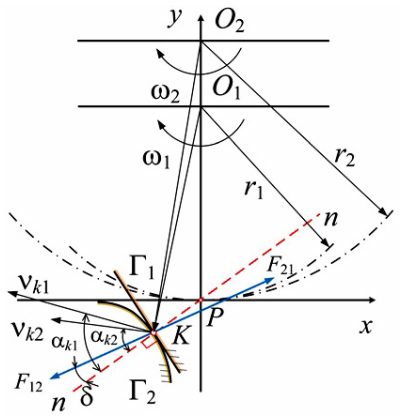

(b)

Fig. 13. Calculation model of meshing efficiency for ACG: (a) before meshing point; (b) after meshing point.

tained, as shown in Fig. 12. The following results are obtained:

(a) μ has a significant effect on the sliding ratio for the ACG pair. Because the value of μ increases, the length of involute tooth profile increases rapidly near the pitch point, so the sliding ratio of the ACG pair will increase.

(b) Near the pitch point (x = 0), the value of sliding ratio for ACG pair is smaller than that of the cycloidal pair. Moreover, at both ends of the tooth profile, the sliding ratio of the ACG is equal to that of the cycloidal gear.

As mentioned, α mainly affects the sliding ratio of the tooth profile for the ACG near the pitch circle, while μ influences the sliding ratio of the whole tooth profile of the ACG. (1) Compared with involute drive, at both ends of tooth profile, the value of sliding ratio for the ACG drive is constant and smaller, and the wear of the tooth profile is also more uniform. (2) Compared with cycloidal gear, the change rate of sliding ratio for the ACG drive is smaller near the pitch point, which makes the drive operate smoothly and have a long wear life.

5.3 Meshing efficiency

(1) Meshing efficiency model. The estimation of the meshing efficiency of gear is an important point in gear transmission design. At the design stage, accurate analysis and evaluation of gear meshing efficiency is helpful to improve the performance of gear transmission and reduce its power loss [29]. The meshing efficiency of the ACG is the ratio of the input power of the driving gear to the power required to overcome the working resistance of the driven gear.

The meshing diagram of the ACG is shown in Fig. 13. The angular velocity of the driving gear is ω_1 and of the driven gear is ω_2. F_{12} is the driving force of the driven gear, F_{21} is the resistance of the driven gear to the driving gear, *n-n* is the normal line of the tooth profile at the meshing point, δ is the angle between the normal line *n-n* and the F_{12}, v_{k1} is the movement velocity of the driving gear at the meshing point, v_{k2} is the movement speed of the driven gear at the meshing point, and α_{k1} and α_{k2} denote the angle between v_{k1} and v_{k2} and the line *n-n*, respectively.

When the ACG pair is meshing before meshing point (K `), the relationship between the position of the conjugate tooth profile is shown in Fig. 13(a). At point K `(x > 0), the input power of the driving gear is obtained by

$$P_1 = F_{12} v_{k1} \cos(\alpha_{k1} + \delta) . \quad (29)$$

The power required to overcome the driven gear resistance is obtained by

$$P_2 = F_{21} v_{k2} \cos(\alpha_{k2} + \delta). \tag{30}$$

According to the plane gear meshing theory, we have

$$F_{12} = F_{21}, \tag{31}$$

$$v_{k1} \cos\alpha_{k1} = v_{k2} \cos\alpha_{k2}. \tag{32}$$

Then, the instantaneous meshing efficiency is obtained by

$$\eta_i = \frac{F_{21} v_{k2} \cos(\alpha_{k2} + \delta)}{F_{12} v_{k1} \cos(\alpha_{k1} + \delta)} = \frac{1 - f \tan\alpha_{k2}}{1 - f \tan\alpha_{k1}} \tag{33}$$

where f is the friction factor, f = 0.1. In the triangles, $\Delta O_1PK`$ and $\Delta O_2PK`$, the values of α_{k1} and α_{k2} can be obtained according to the Cosine theorem:

$$\begin{cases} \alpha_{k1} = \arccos\left(\dfrac{r_1 x}{\sqrt{(y + r_1)^2 + x^2} \cdot \sqrt{x^2 + y^2}} \right) \\ \alpha_{k2} = \arccos\left(\dfrac{r_2 x}{\sqrt{(y + r_2)^2 + x^2} \cdot \sqrt{x^2 + y^2}} \right) \end{cases} x \in [0, x_B). \tag{34}$$

Similarly, when the ACG pair meshes to the point K (x < 0), as shown in Fig. 13(b). The instantaneous meshing efficiency of the ACG is obtained by

$$\eta_i = \frac{F_{21} v_{k2} \cos(\alpha_{k2} - \delta)}{F_{12} v_{k1} \cos(\alpha_{k1} - \delta)} = \frac{1 + f \tan\alpha_{k2}}{1 + f \tan\alpha_{k1}} \tag{35}$$

where, in triangles ΔO_1PK and ΔO_2PK, values of α_{k1} and α_{k2} can be obtained by using the Cosine theorem:

$$\begin{cases} \alpha_{k1} = \arccos\left(\dfrac{-r_1 x}{\sqrt{(y + r_1)^2 + x^2} \cdot \sqrt{x^2 + y^2}} \right) \\ \alpha_{k2} = \arccos\left(\dfrac{-r_2 x}{\sqrt{(y + r_2)^2 + x^2} \cdot \sqrt{x^2 + y^2}} \right) \end{cases} x \in (x_A, 0]. \tag{36}$$

When the ACG pair at pitch point P (x = 0), the ACG pair is equivalent to pure roll, $v_{k1} = v_{k2}$, $\alpha_{k1} = \alpha_{k2}$. According to Eq. (33), the instantaneous meshing efficiency was $\eta_i = 1$.

Furthermore, the instantaneous meshing efficiency of the ACG pair is a function of the rotation angle. Hence, the instantaneous meshing efficiency is integrated by the rotation angle and then averaged to obtain the average meshing efficiency. According to Eqs. (2) and (33), the average meshing efficiency of the ACG pair is obtained by

Table 3. Design parameters of gear drive.

Parameters	μ ($\mu = \mu_1 = \mu_2$)	α
Cycloid gear	0.1	0
ACG-1	0.05	20°
ACG-2	0.05	22.5°
ACG-3	0.05	25°
ACG-4	0.075	25°
ACG-5	0.1	25°
Involute gear	——	25°

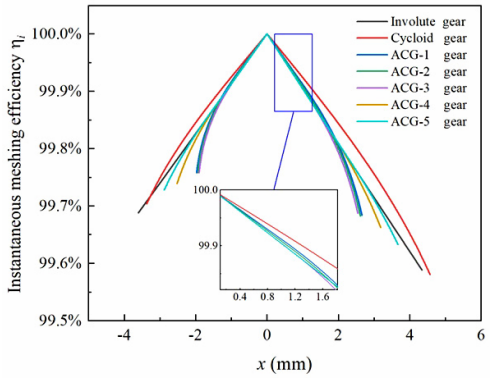

(a)

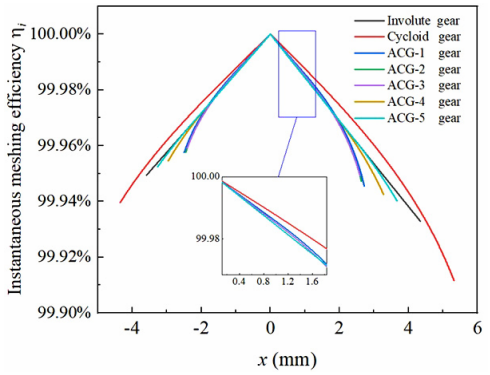

(b)

Fig. 14. Instantaneous meshing efficiency of gear: (a) i = 56/38; (b) i = 56/52.

$$\eta_m = \frac{\int_{\theta_b}^{\theta_a} \eta_i d\theta_1}{\theta_a - \theta_b}. \tag{37}$$

(2) Meshing efficiency analysis. Using the previously described equations, the meshing efficiency of gear transmission is investigated. The main parameters of the numerical examples are listed in Tables 1 and 3. MATLAB software is used for numerical calculation according to Eqs. (2)-(8), (33), and (35). The results of instantaneous meshing efficiency of gear transmission are also obtained, as shown in Fig. 14. Wherein, X-axis represents the abscissa of each point on the contact path.

From Fig. 14, the following results are obtained:

(a) With the increase of value of the x, the instantaneous

meshing efficiency of gear first increases and then decreases, finally reaching the maximum value at the pitch point.

(b) Comparing Figs. 14(a) and (b), when z_1 increases, the instantaneous meshing efficiency of the gear drive increases. However, the increase in transmission ratio will make the instantaneous meshing efficiency of the gear drive decrease.

(c) Compared with involute drive, the instantaneous meshing efficiency of the ACG-5 drive at the position of tooth tip and tooth root (99.73 %, 99.63 %) is close to that of involute gear (99.70 %, 99.58 %), which indicates that the ACG drive has good meshing efficiency.

6. Contact and bending stresses

The contact and bending strength of gear directly affect the service life and safety of the whole mechanical transmission mechanism, so it is necessary to study the contact and bending stresses of the gear drive. Compared with classical mechanical calculation methods, finite element (FE) simulation technology can consider the effect of many factors, such as materials, external environment, and working conditions, so that the calculation result is closer to the real working conditions, and it has been widely used in the calculation of gear contact stress [30]. In this paper, to determine the advantages of the tooth profile of the ACG, we compare the contact and bending stresses of the novel gear and an involute drive. The contact and bending stress of the gear drive are carried out by using the ANSYS Workbench software.

(1) Simulation setup. A number of examples of the ACG-5 and involute gear pairs are provided according to the parameters in Tables 1 and 3. A computerized motion simulation of meshing process is also carried out.

Step 1. According to the mathematical model of tooth profile of the ACG, the set of discrete points of the tooth profile curve is calculated by MATLAB;

Step 2. The discrete points of the tooth profile are imported into SOLIDWORKS for the constructing the 3D geometry model, and the assembled 3D geometry model is imported into ANSYS software for finite element analysis.

Step 3. To reduce the amount of simulation calculation and improve the analysis efficiency, the loading contact simulation is performed for six gear teeth. The driven gear is fully constrained in X, Y, and Z axis directions, the driving gear is fully constrained in X and Y axis directions, and only the rotation degree of freedom in the Z axis direction is retained. The gear tooth mesh unit is a regular hexahedron unit. The number of units and nodes is 151200 and 652974, respectively. The other parameters are shown in Table 4.

The involute drive uses the same set of specifications for comparison.

(2) Bending stress. The results of tooth root bending stress for the ACG and involute drive are shown in Fig. 15. It can be observed that the maximum bending stress of the root of the ACG (47.448 MPa) is 27.078 % less than that of the involute gear (65.067 MPa). This indicates that the ACG with a composite tooth profile design has higher bending strength, which is conducive to the lightweight design of gears. Moreover, both ACG and involute gears have edge contact at the root of the tooth, which is due to the geometric abruptness of the tooth surface at the tooth root, causing drastic changes of stress at the root. Therefore, to eliminate edge contact, the tooth profile modification of the ACG should be carried out.

Table 4. ACG finite element simulation parameters.

Parameters	Values
Material	20CrMnTi
Poisson ratio	0.3
Young's modulus E (GPa)	212
Frictional coefficient	0.1
Output load (N·m)	200
Tooth width B (mm)	15
Input speed (rpm)	100
i	56/52

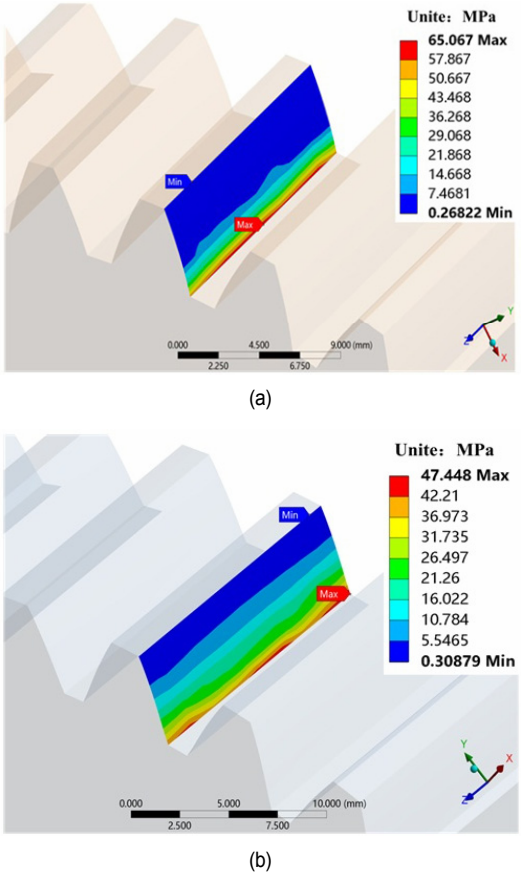

Fig. 15. Bending stress of tooth root: (a) involute gear; (b) ACG.

(3) Contact stress. The results of contact stress for the ACG and involute drive are shown in Fig. 16. It can be observed that in the meshing area, the contact area of the ACG is significantly larger than that of the involute gear, and the contact stress distribution on the tooth surface is relatively uniform and

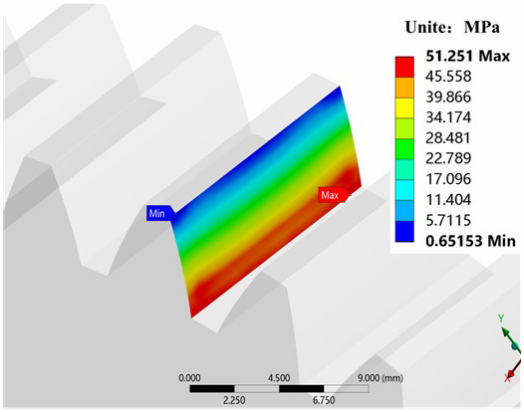

(a)

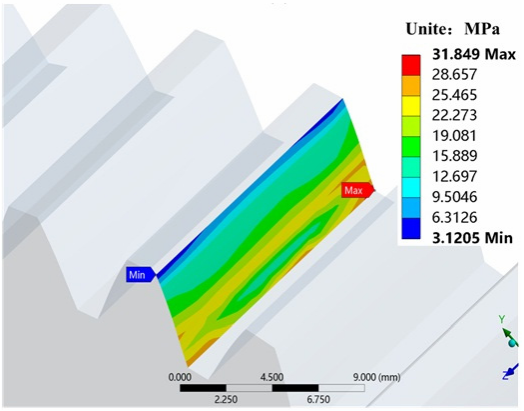

(b)

Fig. 16. Contact stress of tooth surface: (a) Involute gear; (b) ACG.

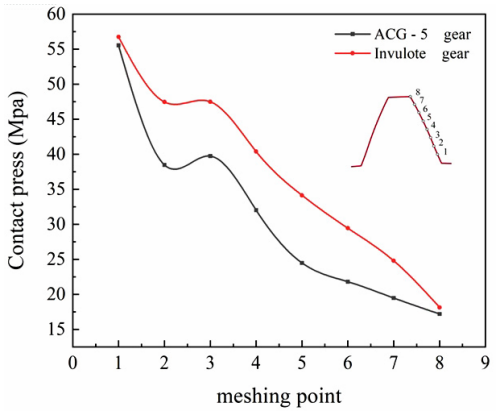

Fig. 17. Dynamic contact stress of the ACG pair.

is banded along the tooth width direction. The maximum contact stress of the ACG and involute gear are 31.849 MPa and 51.251 MPa, respectively. The maximum contact stress of the ACG is reduced by about 37.86 % in comparison with that of involute gear.

In addition, to further analyze the law of contact stress of gear teeth with the rotation angle in one meshing cycle, the dynamic contact analysis of the gear drive is performed, and the results are shown in Fig. 17. It can be observed that the maximum contact stress of both ACG and involute gear occurs at the beginning of the meshing point. The main reason is that when the gear pair starts meshing, the contact area between the tooth surfaces is small, resulting in the contact stress of tooth surface being large. However, compared with ACG, involute gear has a even worse stress concentration problems at the tooth root, especially the contact stress from the contact area to the tooth root is very high. Therefore, application of the tooth profile of the ACG can reduce both bending and contact stresses.

7. Conclusions

Due to the complex over-positioning structure, high manufacturing and assembly accuracy requirements of the RV reducer, innovating a structure and transmission principle is still needed. The ACG reducer proposed in this paper is an attempt in this direction. A new type of tooth profile of ACG is adopted as the transmission teeth of the reducer to improve the comprehensive carrying capacity. The generate principle and contact path of tooth profile of the ACG are described. The mathematical model of tooth profile of the ACG and its overlapping interference are established, and the meshing characteristics of the ACG were also investigated by the numerical calculation and finite element method. The results show that the contact ratio and meshing efficiency of the ACG are close to that of involute gear drive, but the sliding ratio of the ACG is lower and its value is constant at both ends of the tooth profile, which is beneficial to reduce tooth surface wear. Compared with the conventional involute gear pair, the bending and contact stress on the ACG tooth surface are also reduced, which is helpful for gear transmission. The ACG pair without interference can be successfully designed by using the proposed method. The ACG has shown some interesting properties, which indicates that its application in ACG reducer is feasible.

The related investigations on this novel type of gear pair, which include tooth profile modification considering deformation and error, fatigue life of the gear, physical prototype experiments of the reducer, are being carried out or would be the next step of work by the authors. Efforts putting this drive forward into practical application are also needed in the near future.

Acknowledgments

The work was supported by the National Natural Science Foundation of China (Grant No. 51975499 and 51975500). These financial supports are gratefully acknowledged. The authors also sincerely appreciate the comments and modification suggestions made by the editors and anonymous referees.

Nomenclature

a : Center distance of gear pair
B : Tooth width

c^* : Tip clearance coefficient
h_a^* : Addendum coefficient
μ : Dimensionless coefficient
ω_1 : Angular velocity of driving gear
ω_2 : Angular velocity of driven gear
$\boldsymbol{\Gamma}_1$: Tooth surface of driving gear
$\boldsymbol{\Gamma}_2$: Tooth surface of driven gear
r_1 : Pitch radius of driving gear
r_2 : Pitch radius of driven gear
θ_1 : Rotation angular of driving gear
θ_2 : Rotation angular of driven gear
z_1 : Tooth number of driving gear
z_2 : Tooth number of driven gear
Σ_f : Fixed coordinate system
Σ_1 : Movable coordinate system of driving gear
Σ_2 : Movable coordinate system of driven gear
$\overset{\frown}{GA}$: Arc contact path in the third quadrant of coordinate Σ_f
$\overset{\frown}{BH}$: Arc contact path in the first quadrant of coordinate Σ_f
$\overline{GH}$: Straight line contact path of coordinate Σ_f
α : Angle between the line $\overline{GH}$ and the positive X-axis
i_{12} : Transmission ratio
$\overrightarrow{\boldsymbol{v}_1}$: Position vector of driving gear
$\overrightarrow{\boldsymbol{n}_1}$: Normal vector of driving gear
ε : Contact ratio
f : Friction factor
σ : Sliding ratio
η_m : Average meshing efficiency
m : Modulus of gear

References

[1] L. Chen and Z. M. Wang, *Structure and Mechanism of Industrial Robot*, China Machine Press, Beijing, China (2021).

[2] G. L. Li and Y. H. Cui, *Industrial Robot Technology and Application*, Chemical Industry Press, Beijing, China (2019).

[3] W. D. He, X. Li and L. X. Xing, Study on new pin-cycloidal drive with high load capacity and high transmission efficiency, *China Mechanical Engineering*, 16 (7) (2005) 565-569.

[4] F. P. Lu, C. Y. Li, J. Huang and B. K. Chen, Optimization design of RV reducer turning arm bearing, *China Mechanical Engineering*, 31(9) (2020) 1043-1048.

[5] K. Y. Wu, Y. P. Shih and J. J. Lee, Kinematic error analysis of the rotor vector gear reducer with machining tolerances, *J. of the Brazilian Society of Mechanical Sciences and Engineering*, 42 (11) (2020) 566.

[6] L. S. Han, Y. W. Shen, H. J. Dong, G. F. Wang, J. Y. Liu and H. J. Hou, Research on dynamic transmission accuracy for 2K-V-type drive, *Chinese J. of Mechanical Engineering*, 43 (6) (2007) 81-86.

[7] W. S. Lin, Y. P. Shih and J. J. Lee, Design of a two-stage cycloidal gear reducer with tooth modifications, *Mechanism and Machine Theory*, 79 (9) (2014) 184-197.

[8] C. Gorla, P. Davoli, F. Rosa, C. Longoni, F. Chiozzi and A. Samarani, Theoretical and experimental analysis of a cycloid speed reducer, *J. of Mechanical Design*, 130 (11) (2008) 112604.

[9] M. Blagojevic, N. Marjanovic, Z. Djordjevic, B. Stojanovic and A. Disic, A new design of a two-stage cycloidal speed reducer, *J. of Mechanical Design*, 133 (8) (2011) 85001.

[10] C. F. Hsieh, The effect on dynamics of using a new transmission design for eccentric speed reducers, *Mechanism and Machine Theory*, 80 (10) (2014) 1-16.

[11] X. X. Sun, L. Han, K. W. Ma, L. Y. Li and J. Wang, Lost motion analysis of CBR reducer, *Mechanism and Machine Theory*, 120 (2) (2018) 89-106.

[12] M. W. Park, J. H. Jeong, J. H. Ryu, H. W. Lee and N. G. Park, Development of speed reducer with planocentric involute gearing mechanism, *J. of Mechanical Science and Technology*, 21 (8) (2007) 1172-1177.

[13] C. Lin, X. G. Xia and P. L. Li, Geometric design and kinematics analysis of coplanar double internal meshing non-circular planetary gear train, *Advances in Mechanical Engineering*, 10 (12) (2018) 168781101881891.

[14] L. Z. Xu and X. M. Yang, Relative velocity and meshing efficiency for a novel planar ball reducer, *Mechanism and Machine Theory*, 155 (1) (2021) 104057.

[15] Y. Z. Wang, S. Y. Ren and Y. Li, Design and manufacturing of a novel high contact ratio internal gear with a circular arc contact path, *International J. of Mechanical Sciences*, 153-154 (4) (2019) 143-153.

[16] L. Z. Xu, S. Li and W. P. Wang, Sliding ratio for novel cycloidal gear drive, *Proceedings of the Institution of Mechanical Engineers, Part C: J. of Mechanical Engineering Science*, 232 (21) (2018) 3954-3963.

[17] Y. Peng, A. P. Song, Y. H. Shen and X. C. Liu, A novel arc-tooth-trace cycloid cylindrical gear, *Mechanism and Machine Theory*, 118 (12) (2017) 180-193.

[18] Y. Zhou and M. H. Hao, The study of leakage of circular arc–involute-circular arc gear pump, *Advances in Mechanical Engineering*, 9 (9) (2017) 168781401772008.

[19] B. K. Chen, H. Zhong, J. Y. Liu, C. Y. Li and T. T. Fang, Generation and investigation of a new cycloid drive with double contact, *Mechanism and Machine Theory*, 49 (3) (2012) 270-283.

[20] S. M. Luo, J. Y. Mo, J. M. Xu, L. X. Mao and J. M. Fan, *A Type of Abnormal Cycloidal Gear and Abnormal Cycloidal Gear Reducer*, China Patent 110630720A (December 2019).

[21] J. M. Fan, Design and performance analysis of large ratio abnormal cycloidal gear reducer, *Master's Thesis*, Xiamen University of Technology, China (2019).

[22] H. X. Li, W. F. Hou and B. Li, Design of multiple planetary row series transmission controlled by V-slot clutch, *J. of Military Traffic Academy*, 21 (2) (2019) 78-84.

[23] J. Wang, S. M. Luo, D. Y. Su and X. F. Chang, Geometric design and simulation of tooth profile using elliptical segments as its line of action, *J. of Central South University*, 22 (6) (2015) 2119-2126.

[24] F. L. Litvin, *Gear Geometry and Applied Theory*, 2nd ed., Cambridge University Press, Cambridge, UK (2004).

[25] D. Q. Ma, Z. H. Ye, Q. J. Feng and Y. An, Research on contact stress distribution and meshing position change rule of variable hyperbolic cylindrical with arcuate tooth trace, *Manu-*

facturing Technology and Machine Tool, 9 (9) (2019) 53-58.
[26] M. Pleguezuelos, M. B. Sánchez and J. I. Pedrero, Control of transmission error of high contact ratio spur gears with symmetric profile modifications, *Mechanism and Machine Theory*, 149 (7) (2020) 103839.
[27] S. Peng, Z. F. Ma, B. K. Chen, S. L. Qin and S. Y. Wang, Theoretical and experimental investigation on internal gear pair with small sliding ratio, *J. of Central South University*, 25 (4) (2018) 831-842.
[28] L. S. Zhu, L. Xiang and C. Q. Zhou, Wear analysis of gears under dynamic load distribution between gear teeth, *J. of Xi'an Jiaotong University*, 52 (5) (2018) 75-80.
[29] J. C. Yao, Study on a method for Calculating gearing meshing efficiency, *Chinese J. of Mechanical Engineering*, 37 (11) (2001) 18.
[30] J. X. Zhan, M. Fard and R. Jazar, A quasi-static FEM for estimating gear load capacity, *Measurement*, 75 (11) (2015) 40-49.

Jingyu Mo is a doctoral candidate of the School of Aerospace Engineering, Xiamen University, China. His research interests include mechanical design and transmission theory.

Shanming Luo is currently a Professor for the Key Lab of Precision Actuation and Transmission at Jimei University, China. His research interests include mechanical design and transmission theory, kinematics, optimization and manufacturing.

Shengping Fu is currently a Professor at College of Marine Equipment and Mechanical Engineering, Jimei University, China. His research field includes vehicle transmission system dynamics and virtual prototype technology.

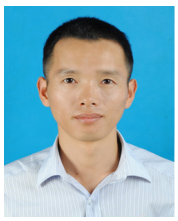

Xuefeng Chang is currently a Professor for the Key Lab of Precision Actuation and Transmission at Jimei University, China. His research interests include design, analysis, detection and manufacture for new type of gear transmission.